

## Microstructure and Fatigue Properties of TiAl with Unique Layered Microstructure Fabricated by Electron Beam Melting

Ken Cho<sup>1,a</sup>, Ryota Kobayashi<sup>1,b</sup>, Takuma Fukuoka<sup>1,c</sup>, Jong Yeong Oh<sup>1,d</sup>,  
Hiroyuki Y. Yasuda<sup>1,e\*</sup>, Mitsuharu Todai<sup>2,f</sup>, Takayoshi Nakano<sup>1,g</sup>, Ayako Ikeda<sup>3,h</sup>,  
Minoru Ueda<sup>4,i</sup> and Masao Takeyama<sup>5,j</sup>

<sup>1</sup>Division of Materials and Manufacturing Science, Graduate School of Engineering,  
Osaka University, 2-1 Yamadaoka, Suita, Osaka, 565-0871, Japan

<sup>2</sup>Department of Environmental Materials Engineering, Institute of Niihama National College of  
Technology, 7-1 Yagumo-cho Niihama, Ehime, 792-8580, Japan

<sup>3</sup>Superalloy Research Group, Research Center for Structural Materials,  
National Institute for Materials Science, 1-2-1 Sengen, Tsukuba, Ibaraki, 305-0047, Japan

<sup>4</sup>Metal Technology Co. Ltd., Harmony Tower 27F, 1-32-2 Honcho, Nakano-Ku,  
Tokyo, 164-8721, Japan

<sup>5</sup>Department of Metallurgy and Ceramics Science, Tokyo Institute of Technology, 2-12-1 Ookayama,  
Meguro-ku, Tokyo, 152-8550, Japan

<sup>a</sup>k\_cho@mat.eng.osaka-u.ac.jp, <sup>b</sup>ryouta.kobayashi@mat.eng.osaka-u.ac.jp,  
<sup>c</sup>takuma.fukuoka@mat.eng.osaka-u.ac.jp, <sup>d</sup>oh@mat.eng.osaka-u.ac.jp,

<sup>e</sup>hyasuda@mat.eng.osaka-u.ac.jp, <sup>f</sup>todai@mat.niihama-nct.ac.jp,

<sup>g</sup>nakano@mat.eng.osaka-u.ac.jp, <sup>h</sup>IKEDA.Ayako@nims.go.jp, <sup>i</sup>mueda@kinzoku.co.jp,  
<sup>j</sup>takeyama@mtl.titech.ac.jp

**Keywords:** TiAl, electron beam melting, macrostructure, fatigue

**Abstract.** In Ti-48Al-2Cr-2Nb (at.%) alloys fabricated by electron beam melting (EBM), a unique layered microstructure composed of duplex-like region and equiaxed  $\gamma$  grains ( $\gamma$  bands) is formed at an appropriate process condition. The fatigue behavior of the TiAl alloy fabricated by EBM at an angle ( $\theta$ ) of  $90^\circ$  between the building direction and loading axis was investigated focusing on the layered microstructure and test temperature. At room temperature (RT), fatigue strength at  $\theta = 90^\circ$  is higher than that at  $\theta = 0^\circ$ . In particular, in low-cycle fatigue life region, the fatigue properties at  $\theta = 90^\circ$  without hot isostatic pressing (HIP) are comparable to those of the cast alloys with HIP. The  $\gamma$  bands act as an effective barrier to the crack propagation, resulting in high fatigue strength at RT. On the other hand, the fatigue strength at  $\theta = 90^\circ$  is lower than that at  $\theta = 0^\circ$  in low-cycle fatigue life region at 1023 K, since the  $\gamma$  bands cannot suppress the crack propagation at 1023 K. However, at 1023 K, the fatigue strength at  $\theta = 90^\circ$  in the low-cycle region is similar to that of the cast alloys with HIP, due to the fine grain size after EBM.

### Introduction

Titanium aluminide (TiAl)-based alloys have been used for low-pressure turbines for aircraft jet engine due to their high specific strength, excellent high-temperature (HT) strength and good oxidation resistance [1-3]. However, low ductility at room temperature (RT), poor HT deformability and high reactivity are harmful for their practical application. The alloys are generally fabricated by the precision investment casting [4]. However, coarser grains, shrinkage defects, contamination from the crucible and oxidation during casting are significant concerns. Thus, in order to solve these problems, new fabrication process for TiAl-based alloys is needed.

Recently, electron beam melting (EBM) [5-7] and selective laser melting (SLM) [8,9] which are typical additive manufacturing techniques for metallic materials are found to be favorable for fabricating TiAl-based alloys. These techniques have some advantages: near-net-shape, reduction of material waste and a decrease of lead-time. In particular, EBM has attracted much attention because

of its high energy density, low residual stress and high process speed, compared with SLM. Thus, EBM process is effective in fabricating TiAl-based alloys.

The mechanical properties of TiAl-based alloys depend on their microstructure which can be controlled by heat treatments [10]. In Ti-rich TiAl alloys, the microstructure generally varies with the annealing condition as follows: (1) a fully lamellar structure composed of TiAl ( $\gamma$ ) and  $\text{Ti}_3\text{Al}$  ( $\alpha_2$ ) phases; (2) a duplex structure composed of fine lamellar grains and  $\gamma$  grains; and (3) a near  $\gamma$  structure mainly composed of equiaxed  $\gamma$  grains. It is well known that the coarse fully lamellar structure is suitable for HT fatigue and creep properties, while the fine duplex structure leads to good balance between strength and ductility [10].

In our previous study [11], we have fabricated cylindrical bars of Ti-48Al-2Cr-2Nb (at.%) (48-2-2) alloy by the EBM process. We found that it is possible to fabricate the alloys with a unique layered microstructure by EBM under optimum condition. The layered microstructure consists of a duplex-like region and equiaxed  $\gamma$  grains forming a chain perpendicular to the building direction. This chain of the  $\gamma$  grains is referred to as the  $\gamma$  band, always aligned perpendicular to the building direction, which is closely related to the temperature distribution near the melt pool during the EBM process. The formation mechanism of the layered microstructure is well documented in our previous paper [11]. It is also interesting to note that the mechanical properties of the alloy bars with the layered microstructure is strongly dependent on the angle ( $\theta$ ) between the loading axis and the building direction [11,12]. For instance, the alloy bars fabricated at  $\theta = 45^\circ$  and  $90^\circ$  exhibit a large elongation above 2.0% at RT, while maintaining the yield stress above 550 MPa [11]. The shear deformation occurs preferentially in the soft  $\gamma$  bands, which leads to the excellent RT ductility at  $\theta = 45^\circ$  and  $90^\circ$ , compared with that of the cast alloys. Furthermore, the RT fatigue strength of the alloy bars at  $\theta = 45^\circ$  is comparable to that of the hot isostatic pressing (HIP)-treated cast alloys, even without HIP treatment [12]. However, the fatigue behavior of the alloy bars at  $\theta = 90^\circ$ , which also exhibit large ductility at RT, has not been clarified yet. In the present study, the RT and HT fatigue behaviors of the alloy bars fabricated by EBM at  $\theta = 90^\circ$  were investigated, focusing on the layered microstructure and the fracture surface after the fatigue tests.

## Experimental Procedures

Ar gas-atomized 48-2-2 alloy raw powder with a mean particle diameter of 100  $\mu\text{m}$  (Arcam AB, Sweden) was used in this study. Cylindrical bars of the alloy with a diameter of 10 mm and a length of 90 mm were fabricated using an Arcam A2X EBM system (Arcam AB, Sweden) at  $\theta = 0^\circ$  or  $\theta = 90^\circ$ . Hereafter, the alloy bars fabricated at  $\theta = 0^\circ$  and at  $\theta = 90^\circ$  are referred to as  $\theta = 0^\circ$  and  $\theta = 90^\circ$ , respectively. The detail of the EBM process is documented in a previous paper [11]. Note that the alloy bars used in this study were not subjected to any post-process treatment including HIP.

The fatigue specimens with gauge dimension of  $2 \times 2 \times 5$  mm were cut from the center of the alloy bars by electro-discharge machining followed by mechanical polishing. The fatigue tests were performed using an electro-servo-hydraulic testing machine at RT and 1023 K in vacuum. The test conditions were set at a frequency ( $f$ ) of 10 Hz and a stress ratio ( $R$ ) of  $-1$  under a fixed applied stress ( $\sigma$ ). Note that the loading axis was set parallel to the cylindrical direction during the fatigue tests. The experimental procedure for the observation of the microstructure and fracture surface using an optical microscope (OM) and scanning electron microscope (SEM) is well described in our previous paper [12].

## Results and Discussion

Fig. 1 shows the microstructure of the alloy bars fabricated by EBM at  $\theta = 0^\circ$  and  $\theta = 90^\circ$ . These OM images were taken from longitudinal plane of the alloy bars. As shown in Fig. 1 (a) and (b), the layered microstructure consisting of the fine duplex-like region and the  $\gamma$  bands can be seen in both  $\theta = 0^\circ$  and  $\theta = 90^\circ$ . The width ( $W_\gamma$ ) and volume fraction ( $f_\gamma$ ) of the  $\gamma$  bands for  $\theta = 0^\circ$  evaluated from OM and SEM images are approximately  $30\ \mu\text{m}$  and 27%, respectively, while the corresponding values for  $\theta = 90^\circ$  are approximately  $35\ \mu\text{m}$  and 33%, respectively. This means that the  $\gamma$  bands at  $\theta = 0^\circ$  and  $\theta = 90^\circ$  are similar to each other. As described in a previous paper [11], the repeated local heat treatment in the vicinity of the melt pool during the EBM process is a key factor for the formation mechanism of these  $\gamma$  bands. The average grain size of the duplex-like region for the alloy bars is approximately  $15\ \mu\text{m}$ , which is much finer than that of the cast alloys with HIP treatment ( $50\text{--}500\ \mu\text{m}$ ) [13].

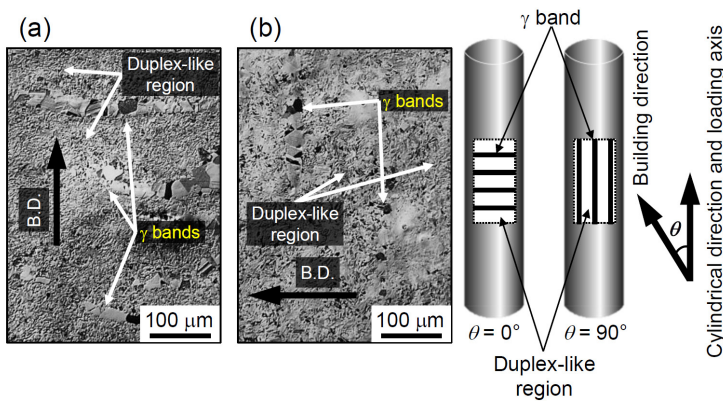


Fig. 1 OM images of  $\theta = 0^\circ$  (a) and  $\theta = 90^\circ$  (b).

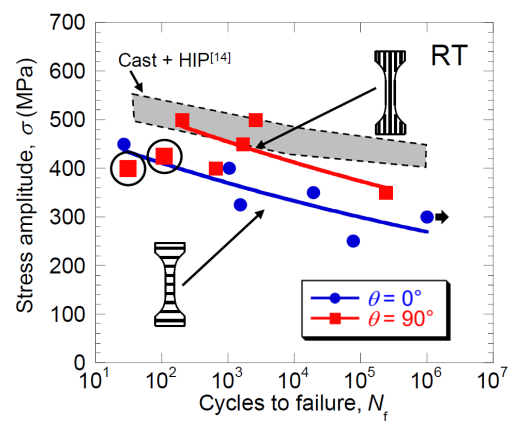


Fig. 2  $S-N_f$  curves of  $\theta = 0^\circ$  and  $\theta = 90^\circ$  cyclically deformed at RT, along with that of the cast alloys with HIP treatment.

The stress amplitude-number of cycles to failure ( $S-N_f$ ) curves of  $\theta = 0^\circ$  and  $\theta = 90^\circ$  cyclically deformed at RT are shown in Fig. 2. The curve for the cast alloys with HIP treatment [14] are also shown in the figure for comparison. Note that  $\theta = 0^\circ$  and  $\theta = 90^\circ$  are not subjected to HIP after the EBM process. As shown in Fig. 2,  $\theta = 0^\circ$  exhibits lower fatigue strength than the cast alloys. On the other hand, the fatigue strength of  $\theta = 90^\circ$  is superior to that of  $\theta = 0^\circ$  and comparable to that of the cast alloys in the low-cycle fatigue life region. However, it should be noted that some of the specimens of  $\theta = 90^\circ$  exhibit shorter fatigue life comparable to that of  $\theta = 0^\circ$  in the same region (marked by circles). This means that the fatigue strength of  $\theta = 90^\circ$  shows a large scatter. It can be deduced that either the main crack initiation at the defect or the change in the crack propagation direction related to the microstructure influences the scatter in the fatigue strength.

In order to understand the variability of the fatigue strength, the fracture surface of the fatigue specimens were observed using a SEM. Fig. 3 shows the SEM fractographs of  $\theta = 90^\circ$  cyclically deformed at  $\sigma = 400\ \text{MPa}$ . It is noted that the specimens shown in Fig. 3 (a) (hereafter specimen A) and (b) (hereafter specimen B) were fractured at 31 cycles and 648 cycles, respectively. This means that specimen B exhibited higher fatigue strength than specimen A. As shown in Fig. 3 (a) and (b), the crack initiation sites can be observed near the specimen surface on both fracture surfaces. Moreover, any defect including pores cannot be seen around the crack initiation sites. These results indicate that the difference in the fatigue strength between specimens A and B is not caused by the defects which accelerate crack initiation during cyclic deformation. However, it should be noted that the relationships between the crack propagation direction and the  $\gamma$  bands in specimens A and B are different from each other, as illustrated in Fig. 3 (c).

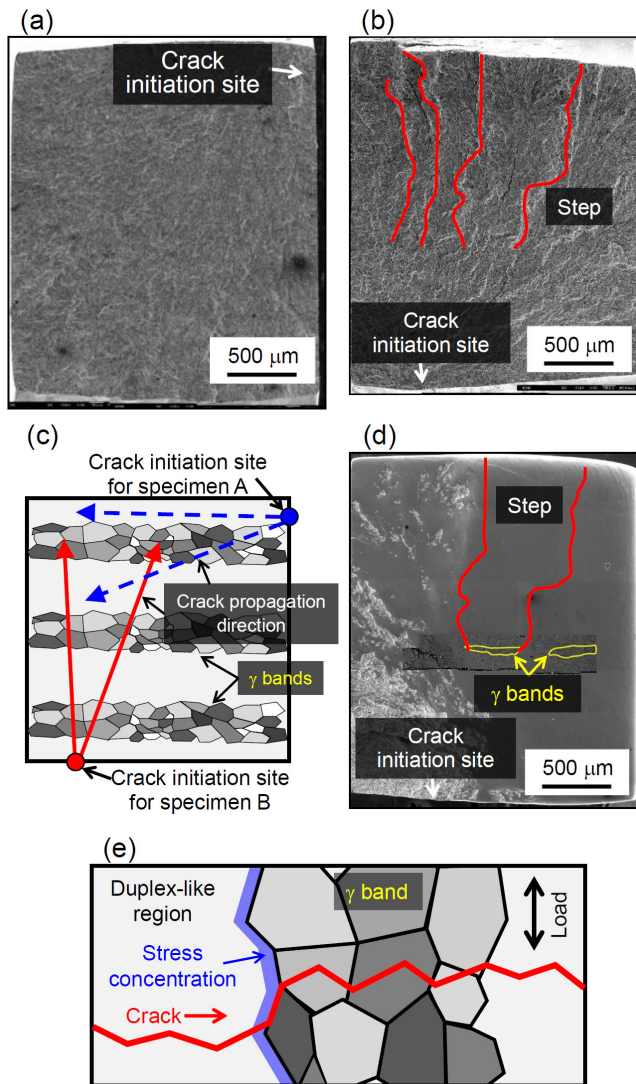


Fig. 3 SEM fractographs after cyclically deformed at RT at  $\sigma = 400$  MPa (a), (b), (d) and schematic drawing of the relationship between the position of the crack initiation site for specimens A and B (e) and crack propagation pass for specimen B (d). (a)  $N_f = 31$  cycles, specimen A, (b)  $N_f = 648$  cycles, specimen B, (d) polished specimen B.

The crack in specimen A initiates near the surface perpendicular to the  $\gamma$  bands. In contrast, the crack initiation site of specimen B positions at the surface parallel to the  $\gamma$  bands. In this way, the direction of crack propagations for specimens A and B are parallel and perpendicular to the  $\gamma$  bands, respectively. It should also be noted that specimen A shows a smooth fracture surface (Fig. 3 (a)), while the fracture surface in specimen B contains some steps (Fig. 3 (b)). Fig. 3 (d) displays the polished fracture surface of specimen B. The  $\gamma$  bands can be observed at the start point of the steps. This indicates that the crack propagation in specimen B was deflected at the  $\gamma$  bands, since the crack propagates perpendicular to the  $\gamma$  bands (Fig. 3 (e)). We reported that the hardness of the  $\gamma$  bands is lower than that of the duplex-like region [11,12]. The difference in hardness between the  $\gamma$  bands and the duplex-like region causes stress concentration at their interface, which leads to the crack deflection at the interface (Fig. 3 (e)). As a result, the crack propagation rate is decreased, and therefore, specimen B exhibits high fatigue strength. In other words, the  $\gamma$  band acts as an effective barrier to the crack propagation at  $\theta = 90^\circ$  at RT if the direction of crack propagation is occasionally perpendicular to the  $\gamma$  bands. In contrast, in specimen A, the crack easily propagates parallel to the  $\gamma$  bands without a strong barrier, resulting in short fatigue life. Thus, the scatter in the fatigue strength of  $\theta = 90^\circ$  at RT is caused by a change in the crack propagation

pass, which depends on the crack nucleation site and the relationship between the direction of crack propagation and the  $\gamma$  bands.

Fig. 4 shows  $S-N_f$  curves of  $\theta = 0^\circ$  and  $\theta = 90^\circ$  cyclically deformed at 1023 K. The  $S-N_f$  curve of  $\theta = 90^\circ$  at 1023 K can be classified into low- and high-cycle fatigue life regions, similar to that of  $\theta = 0^\circ$  [12], which are designated as regions I and II, respectively. It is noted that the fatigue strength of  $\theta = 90^\circ$  is lower than that of  $\theta = 0^\circ$  in region I at 1023 K. Fig. 5 shows SEM fractographs of  $\theta = 90^\circ$  cyclically deformed at  $\sigma = 450$  MPa and then fractured at 440 cycles, which correspond to region I. In contrast to RT, it is difficult to find a clear crack initiation site on the fracture surfaces at 1023 K. As shown in Fig. 5 (b), an intergranular fracture is observed in the  $\gamma$  bands. This means that the  $\gamma$  bands do not act as a resistance for crack propagation at 1023 K. This is because the stress concentration at the duplex-like region/ $\gamma$  band interface is insignificant at 1023 K since the difference in strength between the two regions is decreased at the temperature [11]. The intergranular fracture in the  $\gamma$  bands accelerates the crack propagation rate, thereby decreasing the fatigue strength in region I. Although  $\theta = 90^\circ$  exhibits lower fatigue strength than  $\theta = 0^\circ$  in region I at

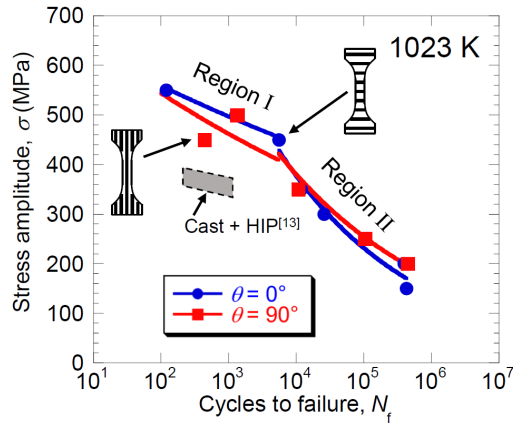


Fig. 4  $S-N_f$  curves of  $\theta = 0^\circ$  and  $\theta = 90^\circ$  cyclically deformed at 1023 K.

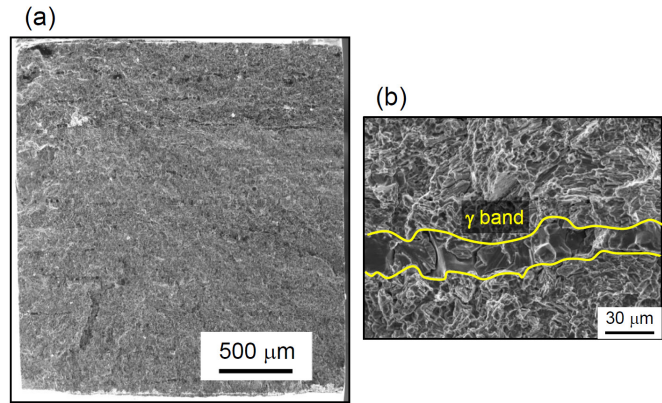


Fig. 5 SEM fractographs of  $\theta = 90^\circ$  after cyclically deformed at 1023 K. (a)  $\sigma = 450$  MPa,  $N_f = 440$  cycles, (b) the  $\gamma$  band observed on the fracture surface.

1023 K, the strength of  $\theta = 90^\circ$  is comparable to or higher than that of the HIP-treated cast alloys [13] because of the fine microstructure. It is also noted that the fatigue strength of  $\theta = 90^\circ$  is comparable to that of  $\theta = 0^\circ$  in region II at 1023 K. The slope of the  $S-N_f$  curve of  $\theta = 90^\circ$  increases in region II, similar to  $\theta = 0^\circ$ . This change in the slope is attributed to the increase in the main and small crack initiations at the pores due to the increase in the stress concentration at the pores associated with low plasticity in region II [12].

## Summary

The RT and HT fatigue behavior of 48-2-2 alloy bars fabricated by EBM at  $\theta = 90^\circ$  without any post-process treatments was investigated with a particular focus on the layered microstructure. The conclusions drawn in this study are given below:

1. The RT fatigue strength of  $\theta = 90^\circ$  is higher than that of  $\theta = 0^\circ$  and comparable to that of the cast alloys with HIP treatment in the low-cycle fatigue life region, even without HIP treatment. This is because the  $\gamma$  band acts as an effective barrier to the crack propagation in  $\theta = 90^\circ$  at RT.
2. However, the fatigue strength of  $\theta = 90^\circ$  shows a large scatter at RT. The variability is caused by the change in the crack propagation pass, which depends on the crack nucleation site and the relationship between the direction of crack propagation and the  $\gamma$  bands.
3. The  $S-N_f$  curve of  $\theta = 90^\circ$  at 1023 K can be classified into low- and high-cycle fatigue life regions, similar to  $\theta = 0^\circ$ . Moreover, the fatigue strength of  $\theta = 90^\circ$  is comparable to that of  $\theta = 0^\circ$  in the high-cycle fatigue life region at 1023 K.
4. The fatigue strength of  $\theta = 90^\circ$  in the low-cycle fatigue life region is lower than that of  $\theta = 0^\circ$ . This is because the  $\gamma$  bands no longer act as a barrier to the crack propagation at 1023 K.

## Acknowledgement

This study was supported by the Cross-Ministerial Strategic Innovation Promotion Program (SIP) "Structural Materials for Innovation" from the Japan Science and Technology Agency (JST).

---

**References**

- [1] Y.-W. Kim, Ordered intermetallic alloys, part III: Gamma titanium aluminides, *JOM* 46 (1994) 30-39.
- [2] Y.-W. Kim, D.M., Dimiduk, M.H. Loretto, *Gamma Titanium Aluminides 1999*, Warrendale, PA, TMS, 1999.
- [3] F. Appel, J.D.H. Paul, M. Oehring, *Gamma Titanium Aluminide Alloys*, Singapore, Wiley-VCH, 2011.
- [4] J. Aguilar, A. Schievenbusch, O. Kätzlitz, Investment casting technology for production of TiAl low pressure turbine blades – Process engineering and parameter analysis, *Intermetallics* 19 (2011) 757-761.
- [5] D. Cormier, O. Harrysson, T. Mahale, H. West, Freeform fabrication of titanium aluminide via electron beam melting using prealloyed and blended powders, *Res. Lett. Mater. Sci.* 2017 (2007) 34737-34740.
- [6] J. Schwerdtfeger, C. Körner, Selective electron beam melting of Ti-48Al-2Nb-2Cr: microstructure and aluminium loss, *Intermetallics* 49 (2014) 29-35.
- [7] M. Seifi, A.A.Salem, D.P. Satko, Ulf. Ackelid, S.L. Semiatin, J.J. Lewandowski, Effects of HIP on microstructural heterogeneity, defect distribution and mechanical properties of additively manufactured EBM Ti-48Al-2Cr-2Nb, *J. Alloys Compd.* 729 (2017) 1118-1135.
- [8] B. Cárcel, A. Serrano, J. Zambrano, V. Amigó, A.C. Cárcel, Laser cladding of TiAl intermetallic alloy on Ti6Al4V – Process optimization and properties, *Phys. Procedia* 56 (2014) 284-293.
- [9] L. Löber, F.P. Schimansky, U. Kühn, F. Pyczak, J. Eckert, Selective laser melting of a beta-solidifying TNM-B1 titanium aluminide alloy, *J. Mater. Process. Technol.* 214 (2015) 1852-1860.
- [10] D.M. Dimiduk, D.B. Miracle, Y.W. Kim, M.G. Mendiratta, Recent progress on intermetallic alloys for advanced aerospace systems, *ISIJ Int.* 31 (1991) 1223-1234.
- [11] M. Todai, T. Nakano, T. Liu, H.Y. Yasuda, K. Hagihara, K. Cho, M. Ueda, M. Takeyama, Effect of building direction on the microstructure and tensile properties of Ti-48Al-2Cr-2Nb alloy additively manufactured by electron beam melting, *Additive Manufacturing* 13 (2017) 61-70.
- [12] K. Cho, R. Kobayashi, J.-Y. Oh, H.Y. Yasuda, M. Todai, T. Nakano, A. Ikeda, M. Ueda, M. Takeyama, Influence of unique layered microstructure on fatigue properties of Ti-48Al-2Cr-2Nb alloys fabricated by electron beam melting, *Intermetallics* 95 (2018) 1-10.
- [13] M. Jouiad, A.L. Gloanec, M. Grange, G. Henaff, Cyclic deformation mechanisms in a cast gamma titanium aluminide alloy, *Mater. Sci. Eng. A* 400-401 (2005) 409–412.
- [14] T. Kruml, M. Petrevec, K. Obrtlík, J. Polák, P. Buček, Influence of niobium alloying on the low cycle fatigue of cast TiAl alloys at room and high temperatures, *Procedia Engineering* 2 (2010) 2297–2305.